Current Biology
Magazine

CellPress

Correspondence

The structure of sperm Izumo1 reveals unexpected similarities with *Plasmodium* invasion proteins

Kaoru Nishimura[1,4], Ling Han[1,4], Enrica Bianchi[2], Gavin J. Wright[2], Daniele de Sanctis[3], and Luca Jovine[1,*]

Fertilization, the culminating event in sexual reproduction, occurs when haploid sperm and egg recognize each other and fuse to form a diploid zygote. In mammals this process critically depends on the interaction between Izumo1, a protein exposed on the equatorial segment of acrosome-reacted sperm, and the egg plasma-membrane-anchored receptor Juno [1,2]. The molecular mechanism triggering gamete fusion is unresolved because both Izumo1 and Juno lack sequence similarity to known membrane fusogens. Here we report the crystal structure of Izumo1, which reveals a membrane distal region composed of a four-helix bundle connected to a carboxy-terminal immunoglobulin (Ig)-like domain through a β-hairpin stabilized by disulfide bonds. Remarkably, different regions of Izumo1 display significant structural similarities to two proteins expressed by the invasive sporozoite stage of *Plasmodium* parasites: SPECT1, which is essential for host cell traversal and hepatocyte invasion [3]; and TRAP, which is necessary for gliding motility and invasion [4]. These observations suggest a link between the molecular mechanisms underlying host cell invasion by the malaria parasite and gamete membrane fusion at fertilization.

Juno and Izumo are structurally unrelated: Juno adopts a modified folate receptor family fold [5], whereas Izumo1 is a type I transmembrane protein consisting of an extracellular region of about 300 residues and a short cytoplasmic tail [2]. The biological activity of Izumo1 depends on the amino-terminal half of its ectodomain — a region named the 'Izumo domain' because it is shared with the paralogous sperm proteins Izumo2, 3 and 4 [6]; this region is followed by a glycosylated Ig-like domain [2] (Figure 1A).

To investigate how Izumo1 might trigger gamete fusion, we expressed the entire ectodomain in mammalian cells and determined a crystal structure to 2.5 Å resolution (Figure S1 in Supplemental Information and PDB ID 5B5K). The structure shows that the Izumo domain consists of a four-helix bundle with a flexible α-helical hook/β-sheet insertion, followed by a β-hairpin that connects the bundle to a seven-stranded Ig-like domain (Figure 1A,B). These features result in an elongated architecture stabilized by five intramolecular disulfide bonds that are conserved in the three Izumo paralogs, and are clearly discernible within the sequence of Spaca6, another sperm surface protein recently reported to be required for gamete fusion [7] (Figure S2A,B). This suggests that the similarity between Izumo1 and Spaca6 is not limited to the carboxy-terminal Ig-like domain, which can be superimposed onto the canonical V-set Ig-like domain of human CD2 (PDB ID 1HNF) — a molecule mediating the adhesion of lymphocytes to antigen-presenting cells — with a root mean square deviation (RMSD) of 2.1 Å over 86 residues.

The helical character of the carboxy-terminal half of the Izumo domain, which corresponds to helices α3 and α4 in our structure (Figure 1A,B), was shown to be important for the function of Izumo1 [6]. The structure readily explains why mutation of leucine residues to proline interferes with this biological activity by disrupting the fold of the four-helix bundle (Figure S2A,C). However, binding assays using peptides representing α3 and α4 suggest that this region of Izumo1 is either not involved in binding to Juno or not sufficient for this interaction (Figure 1C).

Strikingly, structural homology searches revealed a high confidence match between the four-helix bundle of Izumo1 and that of SPECT1, a secreted *Plasmodium* protein that is essential for host cell traversal by the infective sporozoite form of the parasite (Dali Z-score 6.9, RMSD 3.3 Å over 98 residues; Figure 1D). The nearly parallel/antiparallel arrangement of the SPECT1 helical bundle, which also contains a helical hook (albeit inserted at a different position than in Izumo1), has been suggested to adopt a metastable structure which favors the transition from a solvent-exposed to membrane-associated form [8]. In addition, the β-hairpin of Izumo1 is structurally similar to the extensible β-ribbon of TRAP, another *Plasmodium* protein that mediates sporozoite gliding and host cell invasion [4] (RMSD 1.4 Å over 19 residues; Figure 1E). The TRAP β-ribbon is thought to undergo conformational changes upon attachment to host cells and acts as an elbow-like flexible spacer between the amino-terminal α-helical von Willebrand factor A (VWA) domain of the protein (which interacts with the host cell) and its carboxy-terminal β-rich thrombospondin type I repeat (TSR) domain.

What might be the functional implications of the structural similarities to *Plasmodium* cell traversal and invasion proteins with Izumo1? Our findings suggest that the four-helix bundle of the Izumo domain and SPECT1 may orchestrate analogous fusion-related molecular recognition events at the sperm–egg and parasite–host cell interfaces. Izumo1 is not considered a fusogen per se because it cannot induce membrane fusion when heterologously expressed in commonly used cell lines [1]. The presence of solvent-exposed bulk aromatic residues in the Izumo1 four-helix bundle (Figure S2A; a feature also observed in SPECT1) and the report that some monoclonal antibodies that target the Izumo domain do not block binding of sperm to the egg but hinder gamete fusion [6] are consistent with the possibility that an additional, as yet unknown, component is required to form a functional fusogenic complex [9]. Whether SPECT1 is also part of a larger protein complex that could organize proteins that have membrane-disrupting functions, such as SPECT2, is currently unclear [10].

Both SPECT1 and TRAP are expressed by the sporozoite stage

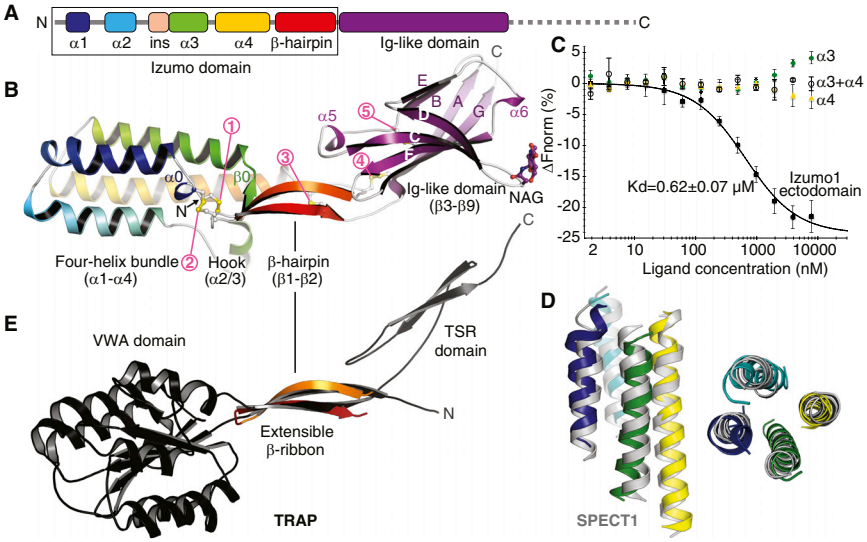

Figure 1. Experimental results and structural comparisons with *Plasmodium* invasion proteins.
(A) Domain architecture of the extracellular region of Izumo1. The Izumo domain, which consists of a four-helix bundle (α1–α4), an insertion (ins: α2/3 hook and β0) and a β-hairpin (β1–β2) — see panel (B) — is boxed. A protease-sensitive carboxy-terminal region that was included in the expression construct used for this study, but is not defined in the electron density map, is indicated by a dashed line. (B) Crystal structure of mouse Izumo1 (amino acids C22–K256), shown in cartoon representation with different regions of the molecule colored as in (A). Amino/carboxyl termini and secondary structure elements are marked. Cysteine residues and the N-acetylglucosamine (NAG) residue attached to N204 are represented in ball-and-stick notation, with circled pink numbers indicating the five disulfide bonds (see also Figure S2A). (C) Microscale thermophoresis experiments show that Juno directly binds to the Izumo1 ectodomain, but does not interact with peptides corresponding to Izumo1 helices α3 and α4 (or an equimolar mixture thereof), which span a region reported to be sufficient for binding to the egg membrane [6]. Vertical error bars represent s.d. of the mean ($n \geq 3$). (D) Structural alignment of the four-helix bundles of Izumo1 and *Plasmodium* SPECT1 (PDB ID 4U5A [8]), in side (left) and top (right) views. Izumo1 helices are colored as in (A,B), SPECT1 is grey. By optimizing the match found by Dali, 84 residues can be superimposed with a RMSD of 3.0 Å. (E) Superposition of the β-hairpin of Izumo1 (red) and the extensible β-ribbon of *Plasmodium* protein TRAP (black; PDB ID 4HQO [4]). Both elements separate amino-terminal α-helical domains from carboxy-terminal β-rich regions in the respective proteins.

of *Plasmodium* parasites and are similarly sequestered within specialized intracellular secretory organelles called micronemes [3,4]. We do not yet know if these proteins, like Izumo1, have a specific binding partner that mediates cell-specific recognition events, or, as has been suggested for sp18 (a five-helical bundle sperm acrosomal protein from the mollusk abalone), are disrupting membrane structure by interacting directly with phospholipids. Nevertheless, it is intriguing that, similar to SPECT1 and TRAP, Izumo1 is sequestered in the acrosome and that its release is also highly regulated by localized secretion.

The structure of Izumo1 provides new mechanistic insights into a fascinating basic biological process and, also considering the protein's recent implication in human immunoinfertility, presents new opportunities in the rational design of new fertility treatments and contraceptives.

SUPPLEMENTAL INFORMATION

Supplemental Information includes two figures and experimental procedures and can be found with this article online at http://dx.doi.org/10.1016/j.cub.2016.06.028.

ACKNOWLEDGEMENTS

We thank R. Aricescu and Y. Zhao (University of Oxford) for the mammalian expression vector pHLsec, and are grateful to T. Shimizu (University of Tokyo) for sharing the coordinates of human IZUMO1 before publication. Access to structural biology beamlines at ESRF is also gratefully acknowledged. Research was supported by Karolinska Institutet; the Center for Innovative Medicine; Swedish Research Council grant 2012-5093; the Göran Gustafsson Foundation for Research in Natural Sciences and Medicine; the Sven and Ebba-Christina Hagberg foundation; an EMBO Young Investigator award; and the European Research Council under the European Union's Seventh Framework Programme (FP7/2007-2013)/ERC grant agreement 260759 (to L.J.); the Wellcome Trust grant number 098051 and the UK Medical Research Council grant MR/M012468/1 (to E.B and G.J.W.).

REFERENCES

1. Bianchi, E., Doe, B., Goulding, D., and Wright, G.J. (2014). Juno is the egg Izumo receptor and is essential for mammalian fertilization. Nature *508*, 483–487.
2. Inoue, N., Ikawa, M., Isotani, A., and Okabe, M. (2005). The immunoglobulin superfamily protein Izumo is required for sperm to fuse with eggs. Nature *434*, 234–238.
3. Ishino, T., Yano, K., Chinzei, Y., and Yuda, M. (2004). Cell-passage activity is required for the malarial parasite to cross the liver sinusoidal cell layer. PLoS Biol. *2*, E4.
4. Song, G., Koksal, A.C., Lu, C., and Springer, T.A. (2012). Shape change in the receptor for gliding motility in *Plasmodium* sporozoites. Proc. Natl. Acad. Sci. USA *109*, 21420–21425.
5. Han, L., Nishimura, K., Sadat Al Hosseini, H., Bianchi, E., Wright, G.J., and Jovine, L. (2016). Divergent evolution of vitamin B_9 binding underlies Juno-mediated adhesion of mammalian gametes. Curr. Biol. *26*, R100–R101.
6. Inoue, N., Hamada, D., Kamikubo, H., Hirata, K., Kataoka, M., Yamamoto, M., Ikawa, M., Okabe, M., and Hagihara, Y. (2013). Molecular dissection of IZUMO1, a sperm protein essential for sperm-egg fusion. Development *140*, 3221–3229.
7. Lorenzetti, D., Poirier, C., Zhao, M., Overbeek, P.A., Harrison, W., and Bishop, C.E. (2014). A transgenic insertion on mouse chromosome 17 inactivates a novel immunoglobulin superfamily gene potentially involved in sperm-egg fusion. Mamm. Genome *25*, 141–148.
8. Hamaoka, B.Y., and Ghosh, P. (2014). Structure of the essential *Plasmodium* host cell traversal protein SPECT1. PLoS ONE *9*, e114685.
9. Inoue, N., Hagihara, Y., Wright, D., Suzuki, T., and Wada I. (2015). Oocyte-triggered dimerization of sperm IZUMO1 promotes sperm-egg fusion in mice. Nat. Commun. *6*, 8858.
10. Ishino, T., Chinzei, Y., and Yuda, M. (2005). A *Plasmodium* sporozoite protein with a membrane attack complex domain is required for breaching the liver sinusoidal cell layer prior to hepatocyte infection. Cell Microbiol. *7*, 199–208.

[1]Department of Biosciences and Nutrition & Center for Innovative Medicine, Karolinska Institutet, Huddinge, SE-141 83, Sweden. [2]Cell Surface Signalling Laboratory, Wellcome Trust Sanger Institute, Hinxton, Cambridge, CB10 1SA, UK. [3]ESRF - The European Synchrotron, Grenoble 38000, France.
[4]Co-first author.
*E-mail: luca.jovine@ki.se

Supplemental Information

The structure of sperm Izumo1 reveals unexpected similarities with *Plasmodium* invasion proteins

Kaoru Nishimura, Ling Han, Enrica Bianchi, Gavin J. Wright, Daniele de Sanctis and Luca Jovine

A

Data Collection	
Wavelength (Å)	0.984
Resolution (Å)	42.3–2.5 (2.59–2.50)
Space group	*I* 4 2 2 (97)
Unit cell (Å, deg)	103.28, 103.28, 139.27, 90, 90, 90
Total reflections	168538 (13122)
Unique reflections	13389 (1304)
Multiplicity	12.6 (10.1)
Completeness (%)	100.0 (100.0)
Mean I/sigma(I)	12.1 (1.1)
Wilson B factor (Å^2)	59.20
R_{pim} (%)	5.7 (75.2)
CC(1/2)	1.00 (0.46)
CC*	1.00 (0.79)
Refinement	
Reflections	13383 (1302)
Free reflections	670 (65)
R_{work} (%)	25.73 (40.20)
R_{free} (%)	28.19 (44.22)
CC_{work}	0.92 (0.45)
CC_{free}	0.88 (0.34)
Number of non–H atoms	1960
Macromolecule	1917
Ligand	15
Water	28
Protein residues	235
RMS deviations	
Bond lengths (Å)	0.004
Bond angles (°)	0.82
Ramachandran plot	
Favored (%)	96.1
Allowed (%)	3.9
Outliers (%)	0
Rotamer outliers (%)	0
Clashscore	4.44 (99th percentile (N=271, 2.50 Å ± 0.25 Å)
MolProbity score	1.52 (99th percentile (N=6960, 2.50 Å ± 0.25 Å)
Average B factor (Å^2)	59.93
Macromolecule	59.58
Ligand	61.04
Water	83.33

B

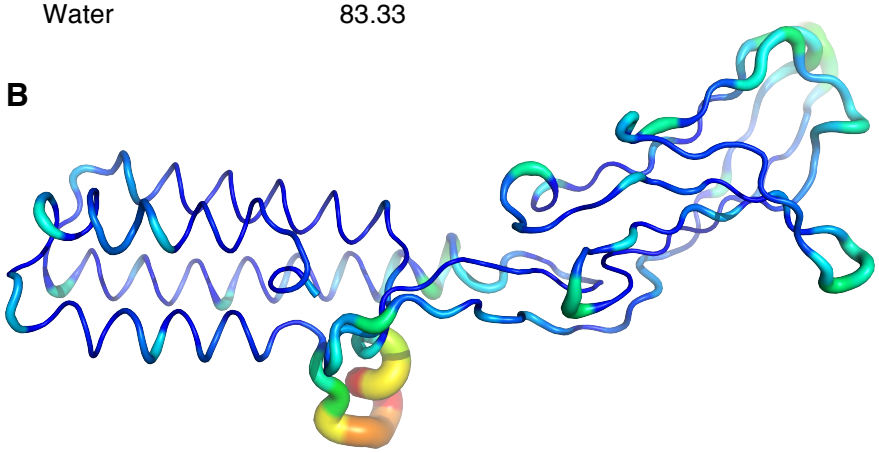

Figure S1. Structure determination of mouse Izumo1.

(A) X-ray data collection and refinement statistics. Values for the outermost shell are shown in parentheses. 100^{th} percentile is the best among structures of comparable resolution, 0^{th} percentile is the worst (for clashscore the comparative set of structures was selected in 2004, for MolProbity score in 2006). (B) Cα atom temperature factor distribution shown in B-factor "putty" representation, using a ribbon radius that increases from lowest (44.09 $Å^2$; dark blue) to highest (146.83 $Å^2$; red) B-factor. With the exception of the α-helical hook region (residues V66-G76), which has an average B-factor of 104 $Å^2$, the bulk of the Izumo1 structure (residues C22-G65, A77-K256) has relatively low and more uniform B-factors (average B-factor 56 $Å^2$). This suggests that, except for the flexible α-helical hook, highly intramolecularly disulfide-bonded Izumo1 is a rigid molecule.

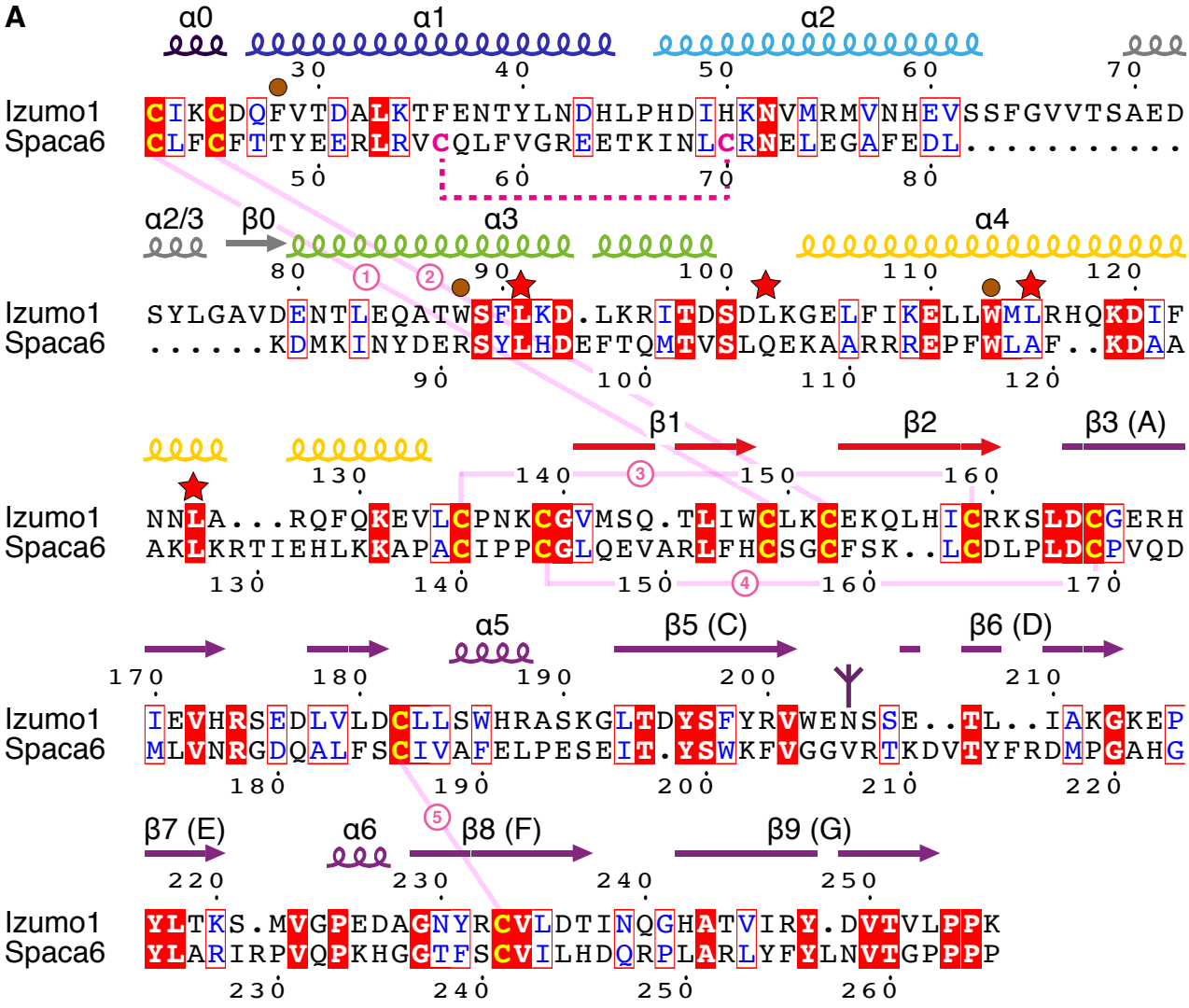
A
α0
α1
α2
Izumo1
Spaca6
α2/3
β0
α3
α4
β1
β2
β3 (A)
α5
β5 (C)
β6 (D)
β7 (E)
α6
β8 (F)
β9 (G)

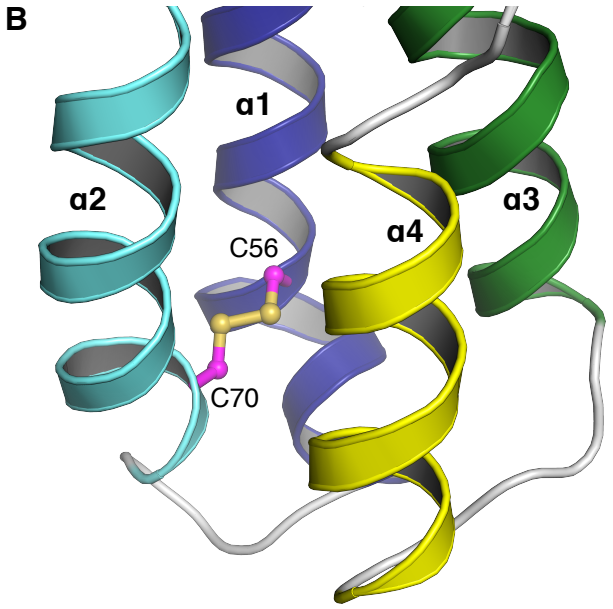
B
α1
α2
α3
α4
C56
C70

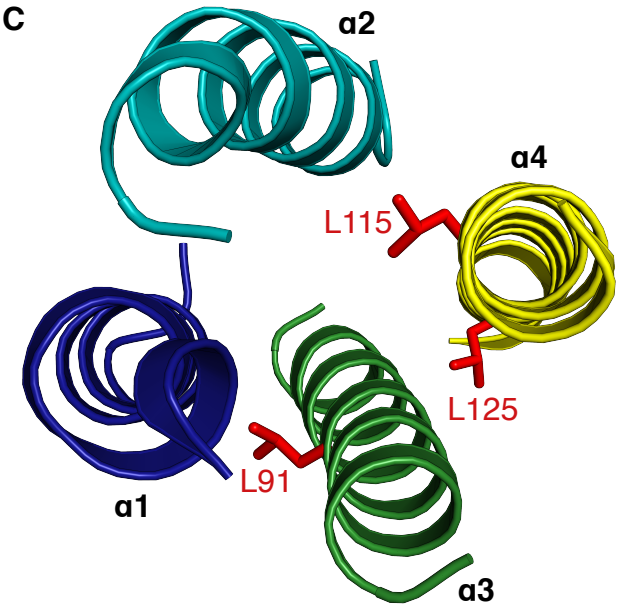
C
α2
α4
L115
L125
L91
α1
α3

Figure S2. The structural features of Izumo1 are conserved in sperm protein Spaca6.

(A) Structure-based sequence alignment of mouse Izumo1 and Spaca6. identical amino acids are white in red boxes, except for cysteine residues that are highlighted in yellow; similar amino acids are blue in white boxes. Secondary structure elements of Izumo1, indicated above the sequences, are labelled and colored as in Figure 1A,B. Conserved disulfide bonds 1-5 are indicated by pink solid lines, and a sixth possible disulfide involving two additional cysteines of Spaca6 (C56 and C70, magenta) is indicated by a dashed magenta line (see also panel (B)). The single N-glycan of Izumo1 is represented by an inverted purple tripod. Izumo domain leucine residues whose combined mutation to proline impairs Izumo1 function ([S1]; panel (C)) are marked by red stars. Solvent-exposed aromatic residues in the four-helix bundle of Izumo1 are indicated by brown circles. (B) Homology modelling shows that the Izumo1 fold is compatible with an additional disulfide bond being formed between C56 and C70 of Spaca6. (C) The structure of Izumo1 clearly shows how the helical bundle fold would be disrupted upon introduction of multiple helix-breaking mutations affecting three leucine residues (red sticks), as well as L102 in the loop between α3 and α4 (not shown) [S1].

SUPPLEMENTAL EXPERIMENTAL PROCEDURES

Protein expression

A cDNA fragment encoding the mouse Izumo1 signal peptide and ectodomain (residues M1-P312) was subcloned into pHLsec3, a mammalian expression vector derived from pHLsec [S2], in frame with a 3' sequence for a LEH_6 affinity tag. The protein was expressed in glycosylation-defective human embryonic kidney 293S cells [S3, S4] (ATCC CRL-3022), deglycosylated with Endoglycosidase H and purified essentially as described [S5, S6].

Protein crystallization and X-ray diffraction data collection

Thin square plate crystals were obtained by sitting drop vapor diffusion at room temperature, using a mother liquor containing 20% (w/v) PEG 3350, 0.2 M ammonium formate pH 6.6. For data collection at 100 K, specimens were cryoprotected using mother liquor supplemented with 10% (v/v) PEG 200, mounted in MicroLoops (MiTeGen) and flash cooled in liquid nitrogen. Data was collected from a single 50 x 50 x 10 µm crystal at European Synchrotron Radiation Facility (ESRF) beamline ID29 [S7], using a PILATUS 6M-F detector (DECTRIS). Integration and scaling were performed with XDS [S8], according to described high resolution cutoff criteria [S9].

Structure determination and refinement

The structure was solved by molecular replacement with Phaser [S10], using the coordinates of human IZUMO1 (PDB ID 5JK9; kindly provided before publication by Prof. Toshiyuki Shimizu, University of Tokyo) as a search model. A single solution was obtained in space group *I*422, with one molecule per asymmetric unit (translation function Z-score: 11.5; log likelihood gain: 86). Correctness of the solution, which packed without any clash, was confirmed by MR-SAD (Molecular Replacement combined with Single-wavelength Anomalous Diffraction phasing) with a dataset collected at λ=1.35 Å from a crystal soaked for 46 h in 0.5 mM uranyl acetate (PHENIX AutoSol BAYES-CC: 53.8 +/- 19.8; FOM: 0.53; overall model-map correlation (101 residues): 0.497; R_{work}/R_{free}: 43%/50%) [S11]. Model building and refinement were performed with Coot [S12] and phenix.refine [S13], using feature-enhanced maps in addition to conventional σA-weighted maps [S14]. Protein geometry was validated with MolProbity [S15], carbohydrate structure validation was carried out using Privateer [S16]. Structure comparisons were performed using the Dali server [S17] and/or the sequence-independent structure-based dynamic programming alignment of PyMOL (Schrödinger); the latter was also used to optimize the superimposition with the Dali SPECT1 hit (Figure 1D). Structural figures were made with PyMOL; the alignment in Figure S2A was prepared using ESPript [S18]. Data collection and refinement statistics are summarized in Figure S1A. Structure factor intensities and atomic coordinates have been deposited in the Protein Data Bank with ID 5B5K.

Homology modeling

A homology model of mouse Spaca6 ectodomain residues C42-P265 [S19] was generated using MODELLER [S20] and energy minimized using YASARA Structure [S21].

Binding affinity determination by microscale thermophoresis

Microscale thermophoresis (MST) analysis [S22] was performed using a NanoTemper Monolith NT.115 instrument (NanoTemper Technologies GmbH). Mouse Juno was fluorescently labelled with a Blue-NHS labelling kit (NanoTemper Technologies GmbH), according to the manufacturer's instructions. The molar ratio of dye and protein was 4:1. Varying concentrations of mouse Izumo1 ectodomain (residues C22-P312, followed by a LEH_6 C-terminal affinity tag) or peptides corresponding to Izumo1 residues D79-K103 and/or G104-L134 (Thermo Fisher Scientific) were titrated against labelled mouse Juno (83 nM) in 20 mM Na-HEPES pH 7.8, 200 mM NaCl, 0.05% (v/v) Tween 20. Samples were loaded into Standard Treated Capillaries (NanoTemper Technologies GmbH) and MST measurements were performed using 20% MST laser power and 20% LED power. Laser-on and -off times were 30 seconds and 5 seconds, respectively. For each set of binding experiments, at least three independent MST measurements were carried out at 495 nm. Datasets were processed with the NanoTemper Analysis software, using the thermophoresis with T jump signal.

SUPPLEMENTAL REFERENCES

S1. Inoue N., Hamada D., Kamikubo H., Hirata K., Kataoka M., Yamamoto M., Ikawa M., Okabe M., and Hagihara Y. (2013). Molecular dissection of IZUMO1, a sperm protein essential for sperm-egg fusion. Development *140*, 3221-3229.

S2. Aricescu A.R., Lu W., and Jones E.Y. (2006). A time- and cost-efficient system for high-level protein production in mammalian cells. Acta Crystallogr. D Biol. Crystallogr. *62*, 1243-1250.

S3. Chang V.T., Crispin M., Aricescu A.R., Harvey D.J., Nettleship J.E., Fennelly J.A., Yu C., Boles K.S., Evans E.J., Stuart D.I. et al. (2007). Glycoprotein structural genomics: solving the glycosylation problem. Structure *15*, 267-273.

S4. Reeves P.J., Callewaert N., Contreras R., and Khorana H.G. (2002). Structure and function in rhodopsin: high-level expression of rhodopsin with restricted and homogeneous N-glycosylation by a tetracycline-inducible N-acetylglucosaminyltransferase I-negative HEK293S stable mammalian cell line. Proc. Natl. Acad. Sci. USA *99*, 13419-13424.

S5. Bokhove M., Sadat Al Hosseini H., Saito T., Dioguardi E., Gegenschatz-Schmid K., Nishimura K., Raj I., de Sanctis D., Han L., and Jovine L. (2016). Easy mammalian expression and crystallography of maltose-binding protein-fused human proteins. J. Struct. Biol. *194*, 1-7.

S6. Han L., Nishimura K., Sadat Al Hosseini H., Bianchi E., Wright G.J., and Jovine L. (2016). Divergent evolution of vitamin B_9 binding underlies Juno-mediated adhesion of mammalian gametes. Curr. Biol. *26*, R100-R101.

S7. de Sanctis D., Beteva A., Caserotto H., Dobias F., Gabadinho J., Giraud T., Gobbo A., Guijarro M., Lentini M., Lavault B. et al. (2012). ID29: a high-intensity highly automated ESRF beamline for macromolecular crystallography experiments exploiting anomalous scattering. J. Synchrotron Radiat. *19*, 455-461.

S8. Kabsch W. (2010). XDS. Acta Crystallogr. D Biol. Crystallogr. *66*, 125-132.

S9. Evans P.R., and Murshudov G.N. (2013). How good are my data and what is the resolution? Acta Crystallogr. D Biol. Crystallogr. *69*, 1204-1214.

S10. McCoy A.J., Grosse-Kunstleve R.W., Adams P.D., Winn M.D., Storoni L.C., and Read R.J. (2007). Phaser crystallographic software. J. Appl. Crystallogr. *40*, 658-674.

S11. Terwilliger T.C., Adams P.D., Read R.J., McCoy A.J., Moriarty N.W., Grosse-Kunstleve R.W., Afonine P.V., Zwart P.H., and Hung L.W. (2009). Decision-making in structure solution using Bayesian estimates of map quality: the PHENIX AutoSol wizard. Acta Crystallogr. D Biol. Crystallogr. *65*, 582-601.

S12. Emsley P., Lohkamp B., Scott W.G., and Cowtan C. (2010). Features and development of Coot. Acta Crystallogr. D Biol. Crystallogr. *66*, 486-501.

S13. Afonine P.V., Grosse-Kunstleve R.W., Echols N., Headd J.J., Moriarty N.W., Mustyakimov M., Terwilliger T.C., Urzhumtsev A., Zwart P.H., and Adams P.D. (2012). Towards automated crystallographic structure refinement with phenix.refine. Acta Crystallogr. D Biol. Crystallogr. *68*, 352-367.

S14. Afonine P.V., Moriarty N.W., Mustyakimov M., Sobolev O.V., Terwilliger T.C., Turk D., Urzhumtsev A., and Adams P.D. (2015). FEM: feature-enhanced map. Acta Crystallogr. D Biol. Crystallogr. *71*, 646-666.

S15. Chen V.B., Arendall W.B., Headd J.J., Keedy D.A., Immormino R.M., Kapral G.J., Murray L.W., Richardson J.S., and Richardson D.C. (2010). MolProbity: all-atom structure validation for macromolecular crystallography. Acta Crystallogr. D Biol. Crystallogr. *66*, 12-21.

S16. Agirre J., Iglesias-Fernandez J., Rovira C., Davies G.J., Wilson K.S., and Cowtan K.D. (2015). Privateer: software for the conformational validation of carbohydrate structures. Nat. Struct. Mol. Biol. *22*, 833-834.

S17. Holm L., and Rosenstrom P. (2010). Dali server: conservation mapping in 3D. Nucleic Acids Res. *38*, W545-9.

S18. Gouet P., Robert X., and Courcelle E. (2003). ESPript/ENDscript: Extracting and rendering sequence and 3D information from atomic structures of proteins. Nucleic Acids Res. *31*, 3320-3323.

S19. Lorenzetti D., Poirier C., Zhao M., Overbeek P.A., Harrison W., and Bishop C.E. (2014). A transgenic insertion on mouse chromosome 17 inactivates a novel immunoglobulin superfamily gene potentially involved in sperm-egg fusion. Mamm. Genome *25*, 141-148.

S20. Webb B., and Sali A. (2014). Comparative Protein Structure Modeling Using MODELLER. Curr. Protoc. Bioinformatics *47*, 5.6.1-32.

S21. Krieger E., Joo K., Lee J., Lee J., Raman S., Thompson J., Tyka M., Baker D., and Karplus K. (2009). Improving physical realism, stereochemistry, and side-chain accuracy in homology modeling: Four approaches that performed well in CASP8. Proteins *77 Suppl 9*, 114-122.

S22. Wienken C.J., Baaske P., Rothbauer U., Braun D., and Duhr S. (2010). Protein-binding assays in biological liquids using microscale thermophoresis. Nat. Commun. *1*, 100.

AUTHOR CONTRIBUTIONS

Conceptualization, K.N., G.J.W, L.J.; methodology, K.N., L.H., D.d.S., L.J.; validation, L.H.; formal analysis, K.N., L.H., D.d.S., L.J.; investigation, K.N., L.H., D.d.S., L.J.; data curation, K.N., L.J.; writing, K.N., G.J.W. and L.J., with comments from L.H, E.B. and D.d.S.; visualization, K.N., L.H., L.J.; supervision, G.J.W, L.J.; project administration, K.N., L.H., L.J.; funding acquisition, G.J.W, L.J.

NOTE ADDED IN PROOF

After acceptance of the present manuscript, two reports describing structural studies of human IZUMO1, JUNO and their complex were published (Aydin *et al.* (2016) Nature *534*, 562-565; Ohto *et al.* (2016) Nature *534*, 566-569).